Development of a Finite Element Methodology for Modelling Mixed-Mode Delamination Growth in Composite Structures

Adrian C. Orifici [* 1], Rodney S. Thomson [2], Richard Degenhardt [3], Sebastian Büsing [4] and Javid Bayandor [1]

[1] *School of Aerospace, Mechanical & Manufacturing Engineering, Royal Melbourne Institute of Technology, GPO Box 2476V, Melbourne, Victoria, 3001, Australia.*

[2] *Cooperative Research Centre for Advanced Composite Structures Limited, 506 Lorimer Street, Fishermans Bend, Victoria, 3207, Australia.*
** corresponding author: r.thomson@crc-acs.com.au*

[3] *Institute of Composite Structures and Adaptive Systems, DLR − German Aerospace Center, Lilienthalplatz 7, 38108 Braunschweig, Germany.*

[4] *Department of Aerospace and Lightweight Structures, RWTH Aachen University, Wuellnerstrasse 7, D-52062 Aachen, Germany.*

Abstract

A critical failure mechanism for composite skin-stiffened structures in compression is separation of the skin and stiffener, which can be considered analogous to interlaminar cracking. This paper presents the extension of a numerical approach developed previously for simulating the propagation of interlaminar cracks in composite structures. The degradation methodology was implemented in MSC.Marc, and involves modelling the structures with shell layers connected by user-defined multi-point constraints (MPCs). User subroutines were written that apply the Virtual Crack Closure Technique to determine the onset of crack growth, and modify the properties of the user-defined MPCs to simulate crack propagation. In previous work, this model was applied only to specimens with Mode I crack growth, and two methods were proposed for handling the release of failing MPCs. In this paper, the model and release methods are extended to handle propagation in any crack growth mode. Numerical results applying the developed methodology are then compared with experimental results of fracture mechanics characterisation tests for Mode II and Mixed Mode I-Mode II. Based on this comparison, the capability of the model to represent delamination growth in any composite structure is demonstrated. Future work will focus on the application of the degradation model for the design and analysis of larger and more complex structures.

Keywords: delamination, Virtual Crack Closure Technique, end notched flexure, mixed mode I-mode II, propagation modelling.

1. Introduction

For stiffened structures in compression one of the most critical damage mechanisms leading to structural collapse is detachment of the skin and stiffener. In co-cured stiffened panels this is caused by delamination growth at or near the skin-stiffener interface, and in secondary bonded panels usually also involves adhesive disbonding between the skin and stiffener. In order to include the effects of skin-stiffener separation in numerical analyses it is necessary to capture both its initiation and propagation. This paper is focused on the growth of an existing skin-stiffener disbond, with the prediction of damage initiation the

subject of separate work [1]. This work is part of the European Commission Project COCOMAT, an ongoing four-year project that aims to exploit the large strength reserves of composite aerospace structures through a more accurate prediction of collapse [2-3].

In structures manufactured from laminated composite materials, skin-stiffener separation can be considered analogous to interlaminar cracking, for which using fracture mechanics to predict crack growth has become common [4-5]. In fracture mechanics, the rate of strain energy released in crack growth is compared to a threshold called the interlaminar fracture toughness G_C. The strain energy release rate G is split into three components for the separate mechanisms of crack growth: opening (I), sliding (II) and scissoring (III). The three modes of G and G_C are usually applied in single-mode criteria or combined in a mixed-mode criterion to determine the onset of propagation.

The Virtual Crack Closure Technique (VCCT) is a common method for determining the components of G along a crack front [6]. The VCCT approach is based on the assumptions that energy released in crack opening equals the work required for crack closure, and crack growth does not change the state at the crack tip. VCCT allows crack growth to be analysed in a single finite element (FE) analysis, and numerous researchers have applied VCCT to analyse a range of structures, including fracture mechanics test specimens [7-8], bonded joints [9-10], and skin-stiffener interfaces [11-13].

Analysing a structure with skin-stiffener separation also requires the disbonded area to be grown during analysis. VCCT has been limited in this respect due to requiring element edge lengths of the order of the ply thickness [14] and needing complicated algorithms to monitor the crack front. An alternative approach is with cohesive elements, which are used to control the relationship between opening stresses and displacements in an interface [15-16]. However, cohesive elements also require a fine mesh to remain accurate, and can become prohibitively inaccurate with larger mesh sizes, making their application to large structures problematic. So, VCCT remains attractive for crack growth analysis as it provides information on the exact nature of the crack front and crack growth mechanisms, and is expected to retain an acceptable degree of accuracy with larger mesh sizes.

In this paper, an approach proposed in previous work [17] based on VCCT for the propagation of interlaminar crack growth in a nonlinear FE analysis is further developed. This approach involves modelling the structure with two layers of shell elements separated by a nominal distance and joined using multiple point constraints (MPCs). At the end of every increment, the strain energy release rates are calculated using VCCT at the MPCs on the crack front. Upon satisfaction of a single or mixed-mode failure criterion any failing MPCs are released, and the disbonded area is increased for the following increment.

In previous work, an approach that attempted to correlate the VCCT assumptions with the crack front created was shown to give more accurate results than a simple fail-release approach for mode I crack growth. In this work, the approach is extended for the analysis of mixed-mode crack growth. Both propagation methodologies are compared to experimental results for end notched flexure (ENF) and mixed-mode bending (MMB) tests. Based on a comparison with the experimental results, recommendations for the future development of the degradation model are made, especially with reference to the goal of developing an approach suitable for the collapse analysis of fuselage-representative structures.

2. Analysis

In the modelling approach developed, nominally coincident shell layers are connected with user-defined MPCs and offset using dummy plies, as shown in Figure 1. The user-defined MPCs are given one of three "states", in order to represent the different constraint conditions within the structure. State 0 is for MPCs in the intact region, state 1 for MPCs in the intact region on the crack front, and state 2 for MPCs in the disbonded region. User subroutines were written to control the MPCs state in order to increase the disbonded area during an analysis. The subroutines were written in Fortran, using the UEDINC and UFORMSN subroutines provided in MSC.Marc (Marc) [18]. The UEDINC user subroutine is called at the end of every increment and calculates the strain energy release rates at all MPCs on the disbond front, then changes the state of any failing MPCs to disbonded for the next increment. The UFORMSN is used to define the constraint matrix for each user-defined MPC, which is set using the state of the MPC. Gap elements are overlaid with the MPCs and are only activated throughout the analysis at the nodes of disbonded MPCs. For further detail on the modelling approach the reader is referred to Ref. 17.

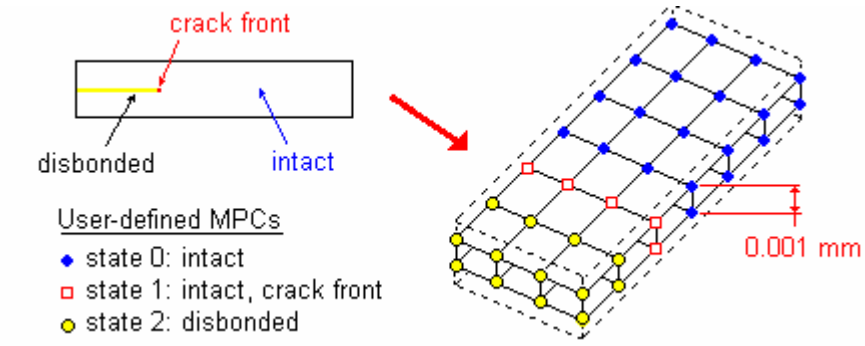

Figure 1: Crack growth modelling with user-defined MPCs

The Virtual Crack Closure Technique was used to determine the strain energy release rates of all MPCs on the crack front. The VCCT equations accounted for arbitrary element sizes, and an algorithm was written to determine the local crack front coordinate system from the neighbouring crack front nodes, following recommendation given in Ref. 14. Separately, a range of different crack front patterns was defined based on the local crack front, and algorithms were written to apply VCCT to each of these patterns by assuming self-similar crack growth. Figure 2 shows an example FE model with arbitrary rectangular shell elements, where the VCCT equations are given by:

$$
\begin{aligned}
G_I &= -\frac{1}{2}\frac{1}{\Delta A} F_{z1}\left(w_2 - w_{2'}\right)\frac{a_0}{a_2}, \\
G_{II} &= -\frac{1}{2}\frac{1}{\Delta A} F_{x1}\left(u_2 - u_{2'}\right)\frac{a_0}{a_2}, \\
G_{III} &= -\frac{1}{2}\frac{1}{\Delta A} F_{y1}\left(v_2 - v_{2'}\right)\frac{a_0}{a_2},
\end{aligned}
\tag{1}
$$

where with reference to Figure 2: G_I, G_{II}, G_{III} are strain energy release rates in local mode I, II and III directions; ΔA is the virtual crack growth area; $\{F_x, F_y, F_z\}$, and $\{u, v, w\}$ are forces and displacements in the local x, y and z directions; a are distances from the crack front MPC; subscripts 0, 1 and 2 refer to values taken from MPCs of states intact, crack front and disbonded, and; 2' is the lower node of the MPC in the disbonded region.

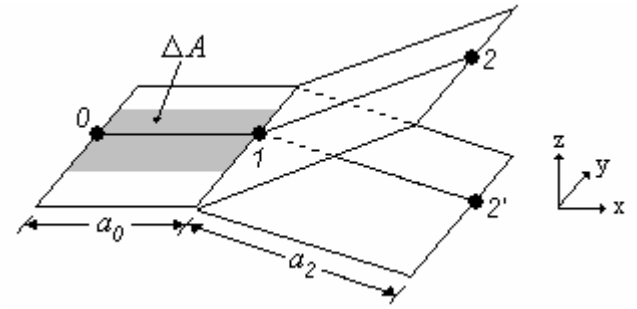

Figure 2: VCCT model with arbitrary rectangular shell elements

For determining the onset of propagation, two mixed-mode failure criteria were implemented, in addition to the option for single-mode criteria implemented previously. The mixed-mode criteria were the Power law and B-K criteria, and are given by:

Power law: $$\left(G_I/G_{IC}\right)^m + \left(G_{II}/G_{IIC}\right)^n + \left(G_{III}/G_{IIIC}\right)^p = 1 \quad (2)$$

B-K: $$\frac{\left(G_I + G_{II} + G_{III}\right)}{\left(G_{IC} + \left(G_{IIC} - G_{IC}\right)\left[\left(G_{II} + G_{III}\right)/\left(G_I + G_{II} + G_{III}\right)\right]^\eta\right)} = 1 \quad (3)$$

where m, n, p and η are experimentally determined curve-fit parameters, and usually $m = n = p = \alpha$ is used. Failure is predicted to occur when the equations are satisfied, and as such the right hand side of the equations is used as a failure index for crack growth.

The propagation method is the way in which the crack front was advanced once the crack growth criteria were satisfied. Two different propagation methods were implemented, outlined in Ref. 17. Propagation Method 1 (PM 1) is a fail-release approach, where each failing MPC is simply released for the next increment. This approach was shown previously to give conservative results in comparison with experimental mode I specimens, as it allowed for the VCCT assumption of self-similar crack growth to be violated. This was due to variations in the crack opening displacements based on the local crack front, and resulted in the energy released upon crack growth not corresponding to the energy calculated using VCCT.

Propagation Method 4 (PM 4, where PM 2 and PM 3 were previously investigated in Ref. 17 and were unsuitable in this work), compares the current local crack front shape with the proposed shape following crack growth, and conservatively adjusts the G values to account for any differences in assumed energy. The crack growth criteria are then reapplied to these adjusted G values and any MPCs no longer failing are removed, and the process is repeated. This approach was previously shown to give more accurate results in comparison with mode I experiments. Developing this approach for mode I crack growth involved an extensive parametric investigation to determine appropriate modification factors, f, based on the local crack front and crack type pattern. In this work, the model was extended to all three modes, which involved similarly extensive parametric studies on nominal mode II and mode III specimens, the results of which are presented in Figure 3. In this, the crack front pattern is the local crack front before growth consisting of a central MPC and up to two neighbouring crack front MPCs (crack types 7, 8 and 9 are on a structural edge), and growth types 1 and 2 correspond to the growth of 1 and 2 of the neighbouring local crack front MPCs. It is worth noting that based on the studies the modification factors for modes II and III were less necessary than those found previously for mode I, particularly in mode II, where many of the factors equalled one.

Crack Type	Growth Type 1 Pattern	f_I	f_{II}	f_{III}	Growth Type 2 Pattern	f_I	f_{II}	f_{III}
1	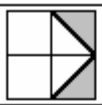	2.5	1.0	1.0 1.5*	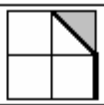	1.5	1.0	1.33 1.0*
2	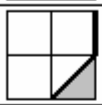	2.0	1.0	1.0	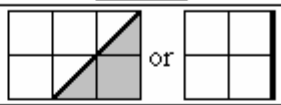	1.0	1.0	1.0
3	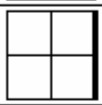	1.5	1.33	1.0		1.33	1.0	1.0
4	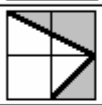	6.0	1.0	2.0	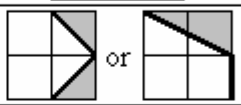	2.0 3.0+	1.0	1.33
5	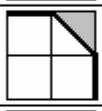	6.0	1.33 1.0*	1.5	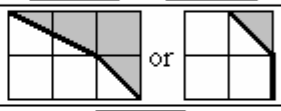	2.0 1.0*	1.0	1.33 1.0+
6	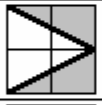	2.0	1.33	2.0	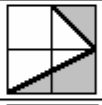	3.0	1.0	1.33 1.0*
7	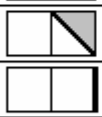	1.33	1.0	1.5	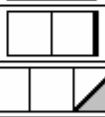	1.0	1.0	1.0
8	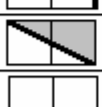	1.33	1.33	1.0	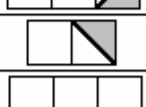	1.0	1.0	1.0
9	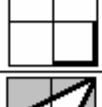	5.0	1.33	1.0		1.0	1.0	1.0
10	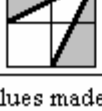	2.0	1.33	1.33	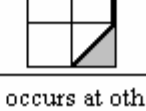	2.0	1.0	1.0
11	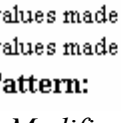	3.0	1.0	4.0 2.0*	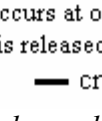	3.0	1.0	1.0

* Choice between values made based on whether crack growth occurs at other MPCs in model
+ Choice between values made based on which crack front node is released

Pattern: intact disbonded crack front

Figure 3: Modification values for PM 4, for each crack front and growth type

3. Results and Discussion

Experimental tests

ENF tests were performed at the German Aerospace Center (DLR) to determine the mode II fracture toughness of the unidirectional carbon fibre prepreg IM7/8552 using the German standard [19,20]. The specimens were cut from previously tested mode I specimens to obtain a mode I pre-crack. Table 1 summarises the specimen details, where "//" is used to denote the location of the delamination within the laminate. Note that in contrast to the unidirectional laminate specified in the standard, a multi-directional laminate was used, as multi-directional laminates find far greater application in aerospace design. A quasi-isotropic lay-up was used that was symmetric about the central 0°//0° interface, to minimise anticlastic curvature, which follows the recommendations given in Ref 21. The ENF test setup is given in Figure 4(a).

Nine ENF specimens were loaded in three-point bending until the onset of crack growth, at which point the test was stopped. The applied load and loading displacement output from the testing machine were used to determine the experimental mode II fracture toughness. There was some scatter in the experimental results, as is typical for ENF specimens [22], though the structural stiffness of all tests was very close. The results for test #2 were close to the average for all specimens, so were used as the basis for comparison with numerical results. The load-displacement graph for specimen #2 is given in Figure 5. For this specimen, crack growth initiated at an applied displacement of approximately 1.43 mm, or 622 N, and the experimental mode II fracture toughness was 517 J/mm.

MMB tests were performed at RWTH Aachen University to investigate the mixed mode I-mode II properties of woven fabric prepreg 950-GF3-5H-1000 using the American standard [23,24]. In the MMB test, shown in Figure 4(b), an end notched specimen is loaded in three-point bending by a central roller that is connected to an end loading hinge, so that the specimen undergoes simultaneous mode II bending and mode I peeling crack opening. The proportion of each loading action, the mixed-mode ratio $G_{II} / (G_I + G_{II})$ or G_{II} / G_T, is controlled by the distance between the load application points, known as the lever arm, c. Three mixed-mode loading ratios were tested, 25%, 50% and 75%, with the corresponding lever arm lengths calculated according the standard, and included with the specimen parameters in Table 1.

Eighteen MMB specimens were tested, consisting of six tests each for 25%, 50% and 75% nominal mixed-mode ratios. MMB specimens were loading in three-point bending until increased loading leads clearly reduction in the reaction load of the specimen, at which point the test was stopped. The applied load and loading displacement output from the testing machine were used to determine the experimental total fracture toughness, which was then split into its components using equations in the standard. The experimental results for all tests showed very good agreement at each mixed-mode ratio, both in terms of the structural stiffness and delamination onset load. The results for test specimens 5.5, 4.3 and 3.1 were close to the average for the 25%, 50% and 75% tests respectively, so were used as the basis for comparison with numerical results. The load-displacement graph for the MMB tests is given in Figure 5. Based on the tests, the experimental fracture toughness values were used to curve-fit coefficients α and η for the Power law (assuming $m = n = p = \alpha$) and B-K criteria. Previous experimental results for pure mode I and mode II tests conducted at RWTH Aachen University on the same material [23] were included in the curve-fitting data, and the results are shown in Figure 6. Note that the experimental mixed-mode ratios for MMB vary slightly from the nominal values.

Table 1: Geometry and material specifications for ENF and MMB tests, dimensions in mm

	ENF	*MMB*
Length, L	100	100
Width	25	25
Pre-crack a_o	30	30
MMB lever arm, c	–	25%: 77.2 50%: 42.1 75%: 30.0
Layup	$[(0,90,+45,-45)_{2S}$ // $(0,90,+45,-45)_{2S}]$	$[0_5$ // $0_5]$
Ply thickness	0.152	0.35
Total thickness	4.864	3.5

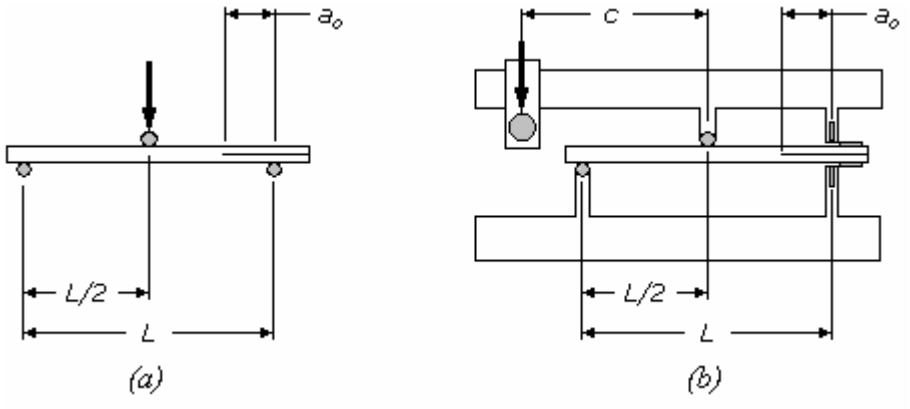

Figure 4: (a) ENF and (b) MMB experimental test setups

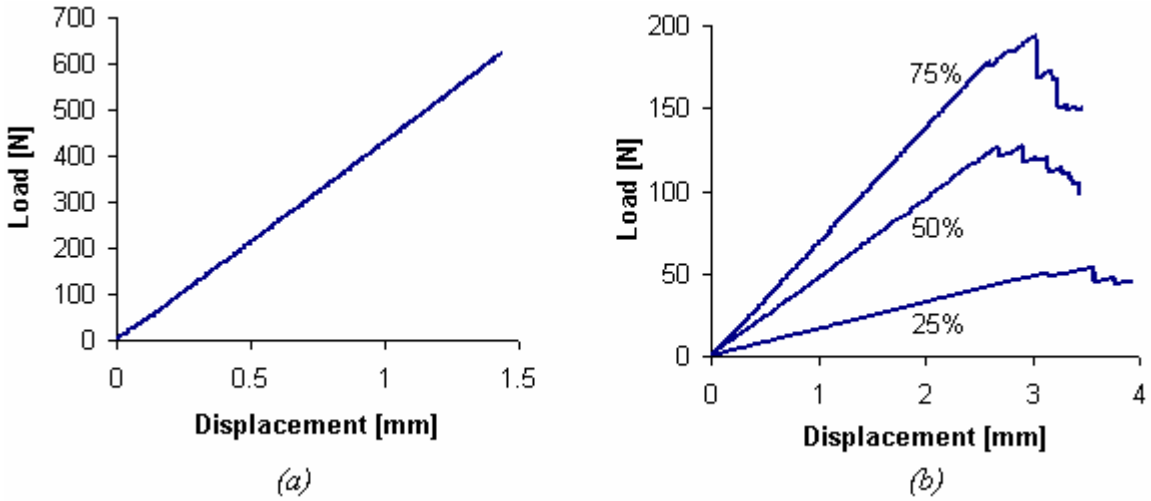

Figure 5: Applied load versus displacement (a) ENF test #2
(b) MMB tests 5.5 (G_{II}/G_T = 25%), 4.3 (G_{II}/G_T = 50%) and 3.1 (G_{II}/G_T = 75%)

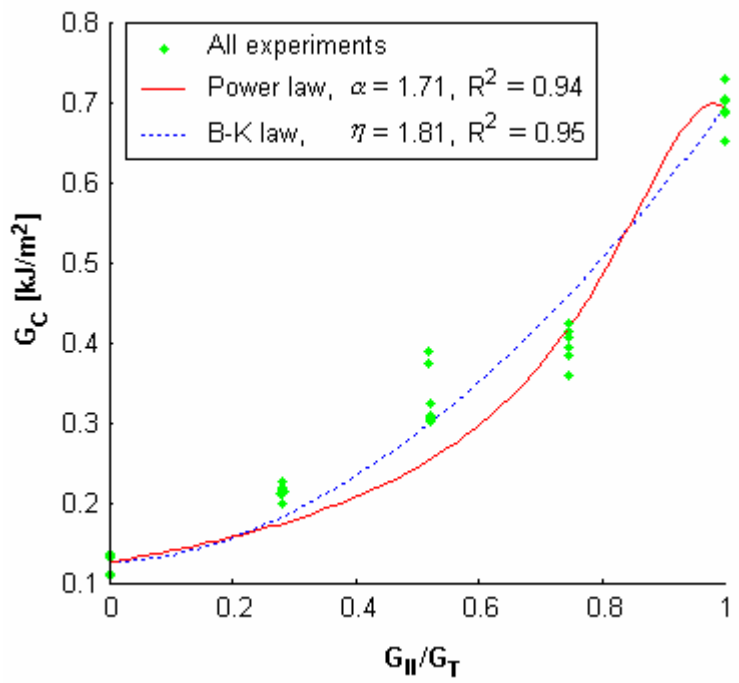

Figure 6: Curve-fitting of fracture toughness values for mixed-mode failure criteria

Numerical analysis

For both the ENF and MMB tests, models were generated at four mesh densities, and were characterised according to the element length in the direction of the crack growth: 5 mm, 2.5 mm, 1.25 mm and 0.125 mm, and are summarised in Figure 7 and Table 2. All models consisted of a pre-crack region of only gap elements between sublaminates, a crack growth region with the user defined MPCs, and the remainder of the structure tied with standard pin-jointed MPCs, where the latter section typically used a coarser mesh than the crack growth region. The support and load application for all models are given in Figure 7, where the MMB loading rig was modelled using rigid links of approximate dimensions. Note that in Figure 7, slight modifications were made to the ENF specimen length and MMB lever arm distance, in order to match the initial experimental stiffness. This can be considered similar to determining the effective support condition, and was necessary so that the boundary condition modelling did not affect the comparison of crack growth prediction.

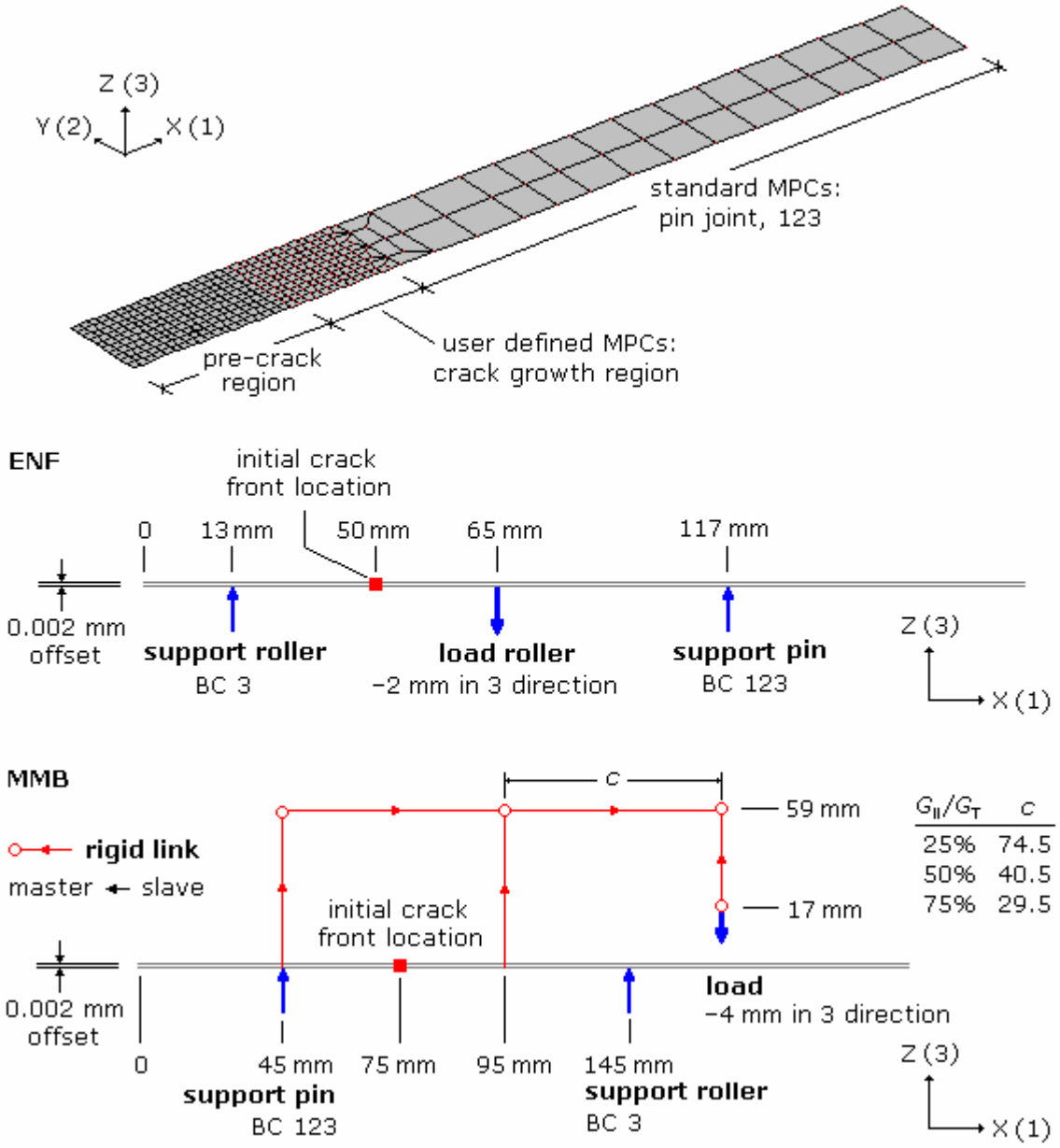

Figure 7: ENF and MMB FE modelling, 2.5 mm model shown in top figure

Table 2: ENF and MMB model details

	ENF				*MMB*			
Model [mm]	**5**	**2.5**	**1.25**	**0.125**	**5**	**2.5**	**1.25**	**0.125**
Nodes	612	798	2846	18,698	466	1660	3638	20,142
Elements	616	1033	4008	27,515	537	2057	4298	19,519
User-defined MPCs	132	132	525	3417	132	462	441	3618
Gap elements	186	341	1344	8991	162	572	903	402

The four mesh density models were run with the two propagation methods and three failure criteria for both ENF and MMB specimens. All models were run on a 2.4 GHz Dual Core AMD Opteron processor using the nonlinear solver in Marc, with a full Newton-Raphson procedure applied and the Marc default tolerance of 0.1 on load residuals. The 5 mm, 2.5 mm and 1.25 mm models were all run for the full displacement loading, while the 0.125 mm models were only run up to a displacement around 0.1 mm past the crack initiation point, to reduce run times due to the increment size being dependent on the element length. Analysis results are presented below, where Figure 8 and Figure 9 are typical comparative curves of applied load versus displacement for the ENF and MMB models, Figure 10 gives the distribution of G along the crack front for both models, and Figure 11 shows the deformed shape and crack length of the MMB 50% model at 3 mm applied displacement.

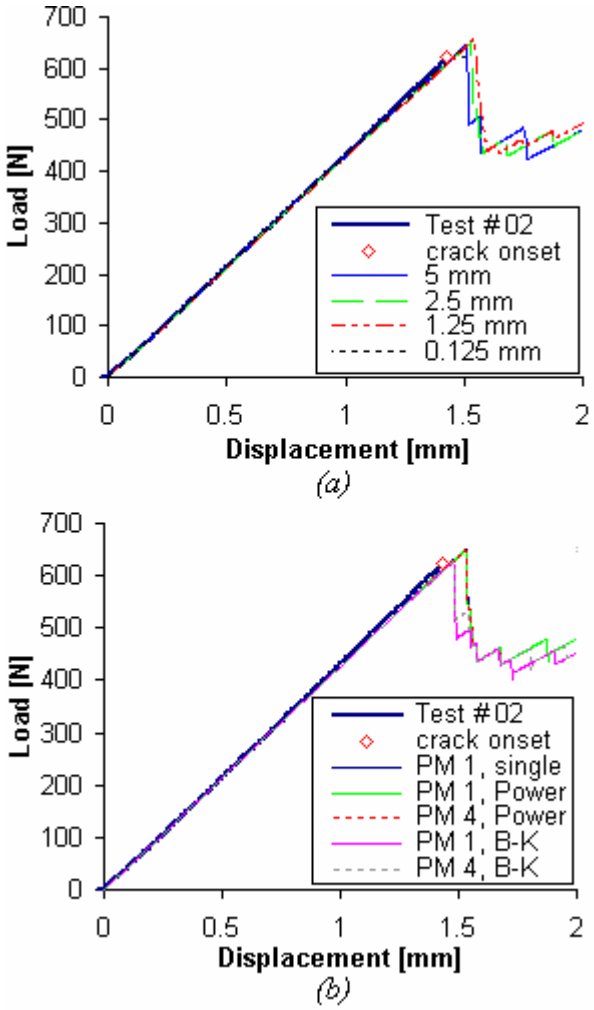

Figure 8: ENF models, applied load versus displacement
(a) PM 1, Power law, varying mesh density (b) varying propagation method

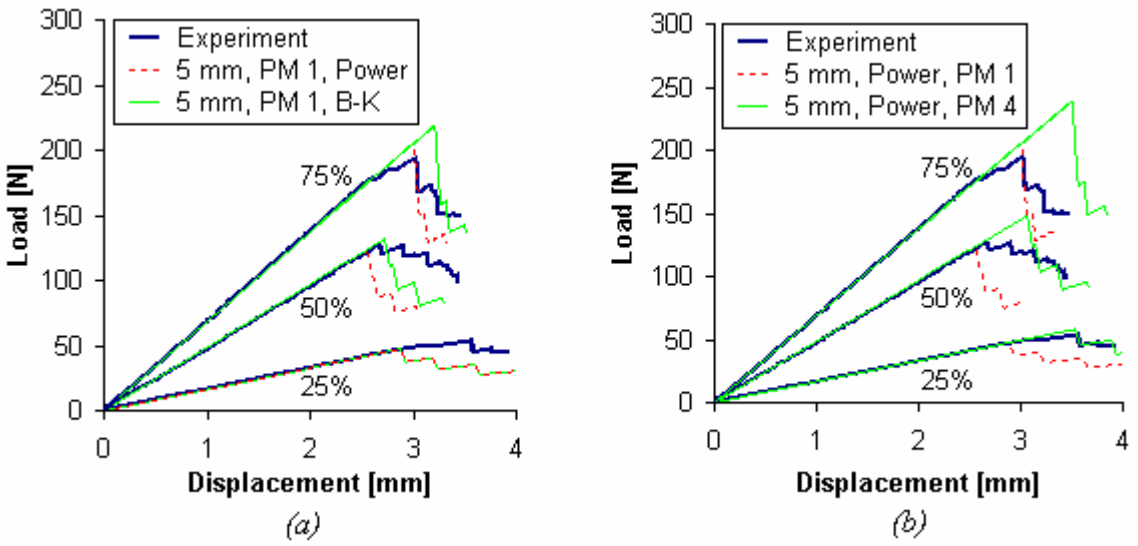

Figure 9: MMB models (varying G_{II}/G_T), applied load versus displacement, (a) varying failure criterion (b) varying propagation method

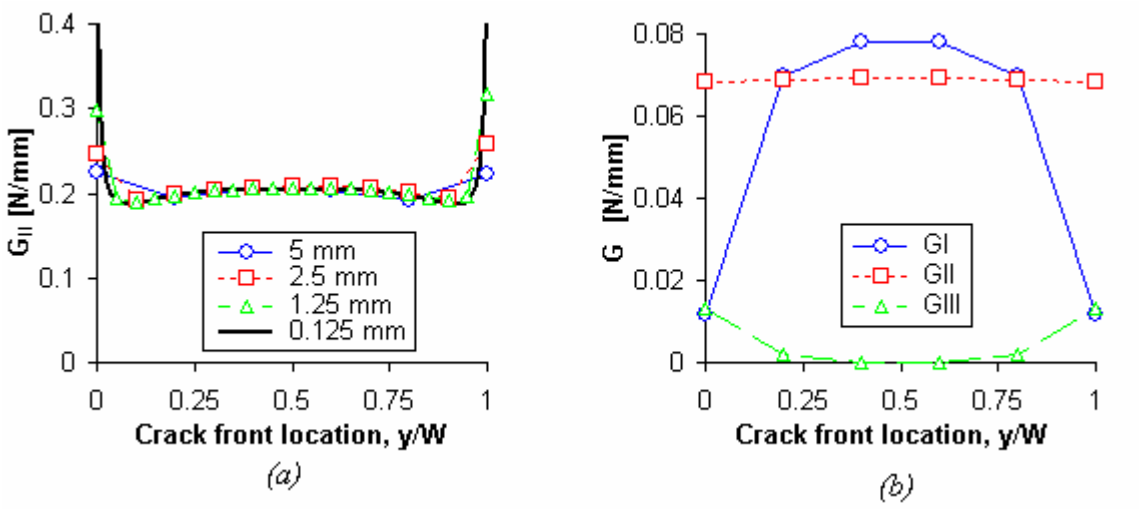

Figure 10: G *distribution along crack front (a) ENF, all models (b) MMB 50% 5 mm*

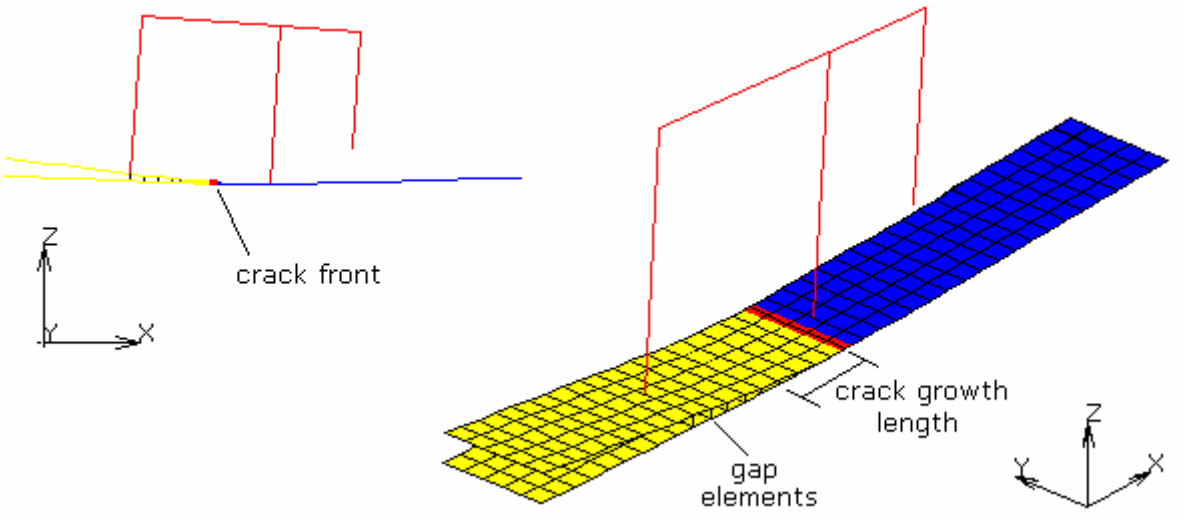

Figure 11: MMB 25% 5 mm model, deformed shape and crack growth, 3 mm displacement

All models displayed similar behaviour regardless of propagation method, which involved an initially linear region leading up to the initiation of crack growth, and crack growth characterised by reductions in the load-carrying behaviour corresponding to advances in the crack front. This behaviour was reflected in the "saw-tooth" appearance of all load-displacement curves, where in general the increasing and decreasing load values corresponded to when the crack front was stationary or advancing. A curved crack front was seen for all models, where the ENF models showed crack growth first occurring at the edges of the specimen, whilst MMB models showed first failure in the specimen centre. This was due to the distribution of G along the crack front, shown in Figure 10, where the variation was due to the anticlastic curvature of the structure, which is a phenomenon for fracture mechanics characterisation tests that is well-known both analytically and experimentally [21,25].

In comparison with the experimental results, all models gave very good predictions of the crack growth initiation as shown in Figure 8 and Figure 9, and were able to represent the specimen behaviour in crack growth. In ENF testing, the applied loading is stopped at the onset of crack growth, due to the prevalence of unstable crack growth [5]. This behaviour was reflected in the FE models, which showed rapid crack growth up to a crack growth length around 17 mm or applied displacement around 1.6 mm, after which crack growth occurred at larger intervals in a more stable manner. For the MMB models, the load-displacement behaviour in crack growth compared well with the experiment, while the failure predictions appeared to be related to the mode-mix ratio, and were more accurate for the 25% models, as shown in Figure 9.

For all models, reducing the element length also required a reduction in the increment size, to ensure that the load was not increased disproportionately to the crack growth. The result of this was that the increase in mesh density doubly penalised the total analysis time due to the increase in both computational expense and required number of increments. However, though the more refined models gave finer detail of the G distribution and crack front shape, the mesh density did not significantly affect the overall structural response and crack propagation behaviour. The application of the different failure criteria had mixed results, with the B-K criterion giving earlier and more accurate predictions of crack growth for the ENF models, though this situation was reversed for the MMB 50% and 75% models, and the two criteria gave identical results for the MMB 25% models.

In terms of the propagation method, PM 1 and PM 4 gave almost identical results for the ENF tests, which is not surprising given that the mode II modification factors were almost all equal to one. For the MMB models, the use of the modification factors in PM 4 resulted in a delay in the failure predictions of around 15%-20% for both the displacement and load at the initiation of crack growth. This modification gave improved predictions for the 25% and 50% models, though led to overestimation for the 75% models. In spite of this, all models showed that the crack opening displacement after crack growth remained largely dependent on the shape of the local crack front, and that the modification factors applied in PM 4 continued to provide a conservative and realistic reduction of the assumed energy released in crack growth.

Discussion

The comparison with experimental results indicated that the accuracy of the failure predictions was dependent on the mixed-mode ratio, where the 75% MMB models overestimated the crack growth initiation while the 25% and 50% models gave accurate or slightly underestimated predictions. This is related to the experimental curve-fit of the Power law and B-K coefficients, where in Figure 6 both criteria over-predicted the G_C data range for the 75% results, whilst under-predicted the 25% and 50% results. In a similar way, the B-K criterion predicted higher G_C values than the Power Law for the range of mixed-mode ratios considered, which corresponded to later predictions of crack growth for all MMB models. This highlights the difficulty in finding a failure criterion that remains accurate across the range of mixed-mode loading conditions, especially considering the variability common in fracture mechanics tests. This is further reinforced by the fact that the coefficients from Figure 6, whilst providing a good fit of the experimental data, could not represent the average experimental result for any of the mixed-mode data sets.

The results of this work have confirmed previous observations that the VCCT approach developed can remain accurate for the predictions of load-carrying capacity with large mesh sizes, which is necessary for its application to aircraft components. Further work will focus on the analysis of "bi-material" interfaces between two dissimilar sublaminates, which occur frequently in stiffened structure design and have been reported by other researchers to affect VCCT calculations accuracy [14]. Separately, an approach to represent the interlaminar damage mechanisms such as fibre fracture and matrix cracking has been developed for application in parallel to the interlaminar damage propagation developed in this paper. This will allow for a more complete analysis of the damage mechanisms acting in composite skin-stiffened structures, and this approach will be further validated and applied using the large amount of experimental results from the COCOMAT project.

4. Conclusion

A method to analyse the propagation of delaminations in composite structures has been developed. The model was implemented for nonlinear finite element analysis using user subroutines in Marc. In the developed approach, user-defined MPCs were applied to control the connection of two shell element layers. At the end of every increment, fracture mechanics calculations were performed using VCCT and any failing MPCs were released for the next increment. Using this approach, the disbonded area could be grown during an analysis and the structural degradation due to disbonding represented.

Numerical predictions using the degradation model with the two propagation methods were compared to experimental results for end notched flexure and mixed-mode bending specimens. In general, close comparison was observed for all aspects of structural behaviour, including the load-carrying capacity, deformation and crack propagation. In terms of the propagation methods, more realistic results were achieved by modifying the strain energy release rate values based on the crack front created in the next increment. This approach was shown to give more accurate results than a simple fail-release approach, as it gave a closer relationship between the assumed and actual energy released in crack growth. Importantly, it was also shown that the use of VCCT with relatively large elements gave almost identical results to even a ply-thickness element length model. The future development of the degradation model was discussed, with reference to the application of the method to the design and analysis of skin-stiffened composite fuselage designs.

Acknowledgments

The authors kindly acknowledge the financial support of: the European Commission, Priority Aeronautics and Space, Contract AST3-CT-2003-502723; the Australian Postgraduate Awards Scheme; the Cooperative Research Centre for Advanced Composite Structures (CRC-ACS); the German Academic Exchange Service, the Italian Ministry of Foreign Affairs, and; the Australian Government under the "Innovation Access Programme – International Science and Technology." The authors would also like to acknowledge Prof. Murray Scott of the CRC-ACS for support within the COCOMAT project.

References

1. A.C. Orifici, I. Herszberg, R.S. Thomson, T. Weller and J. Bayandor, "Failure in stringer interfaces in postbuckling composite stiffened panels," 12th Australian International Aerospace Congress, Melbourne, Australia (2007).
2. R. Degenhardt, R. Rolfes, R. Zimmerman and K. Rohwer, "COCOMAT – Improved **MAT**erial Exploitation at Safe Design of **CO**mposite Airframe Structures by Accurate Simulation of **CO**llapse," Comp. Struct., **73**, 178-178 (2006).
3. COCOMAT Home Page, www.cocomat.de, (2006).
4. T. K. O'Brien, "Characterization of delamination onset and growth in a composite laminate," in: Damage in Composite Materials, ASTM STP 775, 140-167 (1982).
5. T. K. O'Brien, "Interlaminar fracture toughness: The long and winding road to standardization," Comp. B, **29**, 57-62 (1998).
6. E. F. Rybicki and M. F. Kanninen, "A finite element calculation of stress intensity factors by a modified crack closure integral," Eng. Fract. Mech., **9**, 931-938 (1977).
7. R. Krüger, M. König and T. Schneider, "Computation of local energy release rates along straight and curved delamination fronts of unidirectionally laminated DCB- and ENF- specimens," in: Proceedings of the 34th AIAA/ASME/ASCE/AHS/ASC SSDM Conference, La Jolla, CA: AIAA Washington, 1332-1342 (1993).
8. J. Li, S. M. Lee, E. W. Lee and T. K. O'Brien, "Evaluation of the edge crack torsion ECT Test for mode III interlaminar fracture toughness of laminated composites," J. Comp. Tech. Res., **19**, 174-183 (1997).
9. M. M. A. Wahab, "On the use of fracture mechanics in designing a single lap adhesive joint," J. Adhes. Sci. Technol., **19**, 851-865 (2000).
10. M. Qin and Y. Dzenis, "Nonlinear numerical and experimental analysis of single lap adhesive composite joints with delaminated adherends," in: Proceedings of the Thirteenth International Conference on Composite Materials (ICCM13), Y. Zhang, Ed., Beijing (2001).
11. J. T. Wang and I. S. Raju, "Strain energy release rate formulae for skin-stiffener debond modeled with plate elements," Eng. Fract. Mech., **54**, 211-228 (1996).
12. J. Li, T. K. O'Brien and C. Q. Rousseau, "Test and analysis of composite hat stringer pull-off test specimens," J. Amer. Heli. Soc., 350-357 (1997).
13. W. S. Johnson, L. M. Butkus and R. V. Valentin, Applications of Fracture Mechanics to the Durability of Bonded Composite Joints, U.S. Department of Transportation, Federal Aviation Administration DOT/FAA/AR-97/56, (1998).

14. R. Krueger, The Virtual Crack Closure Technique: History, Approach and Applications, NASA/CR-2002-211628, ICASE Virginia, USA (2002).

15. P. P. Camanho and C. G. Dávila, Mixed-mode Decohesion Finite Elements for the Simulation of Delamination in Composite Materials, NASA/TM-2002-211737, NASA Langley Research Center, Virginia, USA (2002).

16. Y. Mi, M. A. Crisfield and G. A. O. Davies, "Progressive delamination using interface elements," J. Comp. Mat., **32**, No. 14, 1246-1272 (1998).

17. A. Orifici, R. Thomson, R. Degenhardt, C. Bisagni and J. Bayandor, "Development of a finite element analysis methodology for the propagation of delaminations in composite structures," in: Proceedings of the XIV International Conference on Mechanics of Composite Materials, Riga, Latvia, 29 May - 2 June (2006).

18. MSC.Marc and MSC.Mentat User Manuals Version 2005r3, MSC.Software Corporation, Santa Ana, CA, (2006).

19. Kling A., Degenhardt R., Characterization of material properties - Results of the EU project COCOMAT, Internal DLR Report, IB 131-2006/18, April 2006.

20. Determination of Interlaminar Fracture Toughness Energy - Mode II - G_{IIC}. European Normative Standard DIN EN 6034, Deutsches Institut für Normung, e. V., 1996.

21. B. D. Davidson, "An analytical investigation of delamination front curvature in double cantilever beam specimens," J. Compos. Mater., **24**, 1124-1137 (1990).

22. A. J. Brunner, "Experimental aspects of Mode I and Mode II fracture toughness testing of fibre-reinforced polymer-matrix composites," Comput. Meth. Appl. Mech. Engrg., **185**, 161-172 (2000).

23. Büsing, S., Reimerdes, H.-G., Investigation of degradation by tests and development of degradation models, COCOMAT Technical Report, RWTH Aachen University, January, 2006.

24. Standard Test Method for Mixed Mode I-Mode II Interlaminar Fracture Toughness of Unidirectional Fiber Reinforced Polymer Matrix Composites, ASTM D6671–01, American Society for Testing and Materials, 2001.

25. B. D. Davidson, "An analytical investigation of delamination front curvature in double cantilever beam specimens," J. Compos. Mater., **24**, 1124-1137 (1990).